Properties of highly crystalline NiO and Ni nanoparticles prepared by high-temperature oxidation and reduction

Mikhail Feygenson,[1] Angela Kou,[1] Lauren E. Kreno,[1] Amanda L. Tiano,[2] Jonathan M. Patete,[2] Fen Zhang,[2] Moo Sung Kim,[1] Vyacheslav Solovyov,[1] Stanislaus S. Wong,[1,2] and Meigan C. Aronson[1,3,*]

[1]*Condensed Matter Physics and Materials Science Department, Brookhaven National Laboratory, Upton, New York 11973, USA*
[2]*Department of Chemistry, Stony Brook University, Stony Brook, New York 11794, USA*
[3]*Department of Physics and Astronomy, Stony Brook University, Stony Brook, New York 11794, USA*

We describe here the use of high-temperature oxidation and reduction to produce highly crystalline nanoparticles of Ni and NiO. Starting with an amorphous Ni powder, we demonstrate that oxidation at 900 °C produces faceted NiO nanocrystals with sizes ranging from 20 to 60 nm. High-resolution transmission electron microscopy measurements indicate near-perfect atomic order, truncated by (200) surfaces. Magnetization measurements reveal that the Néel temperature of these NiO nanoparticles is 480 K, substantially reduced by finite-size effects from the bulk value of 523 K. The magnetization of these faceted NiO nanoparticles does not saturate in fields as large as 14 T while a loop offset is observed which increases from 1000 Oe at 300 K to its maximum value of 3500 Oe at 50 K. We have used high-temperature reduction to transform the faceted NiO nanoparticles into highly ordered Ni nanoparticles, with a Curie temperature of 720 K and blocking temperatures in excess of 350 K. Subsequent efforts to reoxidize these Ni nanoparticles into the core-shell morphology found that the Ni nanoparticles are much more resistant to oxidation than the original Ni powder, perhaps due to the relative crystalline perfection of the former. At 800 °C, an unusual surface roughening and subsequent instability was observed, where 50-nm-diameter NiO rods grow from the Ni surfaces. We have demonstrated that high-temperature oxidation and reduction in Ni and NiO are both reversible to some extent and are highly effective for creating the highly crystalline nanomaterials required for applications such as exchange-bias devices.

I. INTRODUCTION

A fundamental limitation to use ever smaller ferromagnetic particles to increase magnetic-recording density is the tendency of the particle moments to spontaneously reorient since the energy barrier between states with opposite moments is proportional to the particle volume. Exchange coupling to an antiferromagnet is a promising route to stabilize the moment of small ferromagnetic particles and to increase the density of magnetic recording. Currently, devices employing this exchange-bias effect are constructed using elaborate electronic fabrication techniques, and external fields of ~1000 Oe are required to overcome the energy barrier protecting the ferromagnetic moment from spontaneous reversal.[1] Ferromagnetic core/antiferromagnetic shell nanoparticles offer, in principle, many advantages. Simple chemical syntheses provide particles which can be highly monodisperse, and offer a high degree of control over the core and shell dimensions, needed to optimize the exchange-bias field H_{EB} itself. Indeed, H_{EB} can approach values as large as 1 T in Co/CoO core-shell nanoparticles,[2–7] testifying to the low degrees of disorder possible in these simple binary systems, and the extent to which the interface magnetic structure can be manipulated by external chemical treatments such as oxidation.[7] The exchange-bias effect can only be observed below the Néel temperature of the antiferromagnetic shell, which is no larger than the bulk value of 293 K in CoO. Thus, Co core/CoO shell nanoparticles are not suitable for use in magnetic-recording devices which operate at room temperature.

The system Ni/NiO potentially bypasses this fundamental limitation since the Néel temperature of bulk NiO is 523 K. However, studies on Ni-NiO systems have so far found a relatively small H_{EB}, present only at the lowest temperatures.[8] It is well established that one of the most important factors affecting the exchange-bias effect is the overall roughness of the ferromagnetic/antiferromagnetic interface,[9–12] which is controlled by the overall crystallinity of the core and shell in magnetic nanoparticles. It is possible that this crystallinity could be improved by self-annealing, where the Ni and O ions rearrange into a defect-free structure. This degree of ionic mobility can only be realized during the initial formation of the nanoparticles in solution, and subsequently at temperatures which approach the melting point of the nanoparticles themselves. There has been relatively little study so far of the high-temperature processing of nanoparticles,[13–15] and its viability as a method for improving nanocrystallinity and consequently increasing the exchange-bias effect in the Ni/NiO system has not been investigated.

We describe here a procedure by which simultaneous oxidation and coalescence at temperatures of 800−900 °C transforms amorphous Ni powder into highly crystalline NiO nanoparticles. Our magnetic measurements find that a measurable exchange-bias effect is only found in the initial stages of this process, indicating that the core/shell structure is never fully realized. We further show that it is possible to transform the NiO nanocrystals into Ni nanocrystals by high-temperature reduction, and that the Ni nanocrystals can subsequently be reoxidized, potentially opening the door to

custom-tailored layering of ferromagnetic Ni and antiferromagnetic NiO in a single nanoparticle. Although we conclude that the nanocrystals which we synthesized were ultimately too large to support a measureable exchange-bias effect, this research indicates that high-temperature self-annealing is quite effective for producing the highly crystalline Ni and NiO nanoparticles required for a large exchange-bias effect.

II. EXPERIMENTAL DETAILS

The starting point for this study was a nanograined Ni powder. Our synthesis of Ni nanoscale powder was adapted from a modified polyol route, previously presented, starting from nickel chloride as the precursor and sodium borohydride as the reducing agent.[16] Ethylene glycol (VWR, 99.0%), $NiCl_2 \cdot 6H_2O$ (Baker, 98.0%), $NaBH_4$ (Alfa Aesar, 98%), acetone (VWR, 99.9% min), and absolute ethanol (Acros Organics, 200 Proof) were all utilized as purchased, without further purification. In a typical synthesis, 5.1 mmol of $NiCl_2 \cdot 6H_2O$ was dissolved in 30 mL of ethylene glycol and was refluxed to 140 °C under constant stirring, so as to dissolve the precursor, resulting in a green-colored solution. At 140 °C, 25.6 mmol of $NaBH_4$ was added to the reaction flask to reduce Ni^{2+}, resulting in an immediate color change from green to black, though the colloidal dispersion remained stable. The system was maintained at 140 °C under constant stirring for 2 h, after which it was allowed to cool to room temperature. A black precipitate was eventually separated from solution by centrifugation to remove ethylene glycol followed by subsequent washing twice with aliquots of ethanol and acetone, respectively, prior to isolation.

The powder was subsequently heated to temperatures as large as 900 °C, both in air and in an Ar 95%/H 5% mixture. Differential thermal analysis (DTA) was performed from room temperature to 1000 °C using a Labsys Setaram DTA while thermogravimetric analysis (TGA) was performed over a similar temperature range with a TA Instruments TGA Q500. The crystal structures of the powders, both as grown and at different stages in the heat treatments, were determined with a Scintag powder x-ray diffractometer using Cu $K\alpha$ radiation. Transmission electron microscopy (TEM) was carried out using FEI Bio TwinG2 transmission electron microscope equipped with an AMT XR-60 charge-coupled device digital camera system. Magnetization measurements were carried out at temperatures from 10 to 350 K and in fields as large as 7 T using a Quantum Design magnetic property measurement system, and at temperatures from 300 to 800 K and fields as large as 14 T using a vibrating sample magnetometer in a Quantum Design physical property measurement system. The samples were contained in gelatin capsules fastened in plastic straws for immersion into the magnetometer. No glass wool or epoxy were used during the measurements. In all cases, magnetization is normalized per gram of sample. In the case of the starting Ni material, this includes the weight of attached ethylene glycol but reflects the total weight of Ni and NiO components of the oxidized and reduced samples.
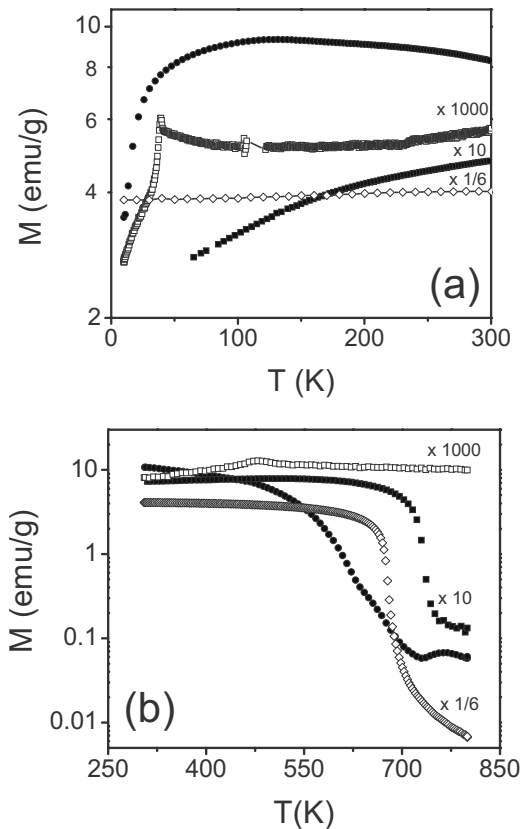
FIG. 1. A comparison of the temperature-dependent dc magnetization for different samples which were zero-field-cooled, and subsequently measured in a fixed field of 1000 Oe. Ni protomaterial (●), protomaterial after 3 days oxidation at 400 °C (■) and 900 °C (□) and faceted Ni nanocrystals prepared by reducing NiO crystals (◇). (a) Low-temperature magnetization scaled by different factors to emphasize their different temperature dependencies and (b) high-temperature magnetization.

III. RESULTS AND DISCUSSION

Our analysis of the Ni starting material indicates that its behavior is much as would be expected for a fine-grained ferromagnet, and that almost no crystalline order is present. The as-grown Ni material was cooled in zero field, and its magnetization M was then measured in a 1000 Oe field with increasing temperature. As shown in Fig. 1(a), typical superparamagnetic behavior is observed, indicating a blocking temperature of ~100 K and the onset of ferromagnetic order itself at 700 K, reasonably close to the 627 K Curie temperature of bulk Ni [see Fig. 1(b)]. X-ray diffraction measurements [Fig. 2(a)] concur that the Ni starting material has the fcc structure and lattice constants of bulk Ni, although the breadth of the diffraction peaks indicates that crystalline order is restricted to length scales smaller than 1 nm. TEM experiments [Fig. 3(a)] show that the as-grown Ni particles have an indeterminate morphology, perhaps best described as polycrystalline over a broad range of length scales. Taken together, our measurements indicate that our starting material has no well-defined nanoparticles but is instead best described as fine-grained or amorphous Ni. The most likely explanation is that the nucleation of the Ni nanoparticles in
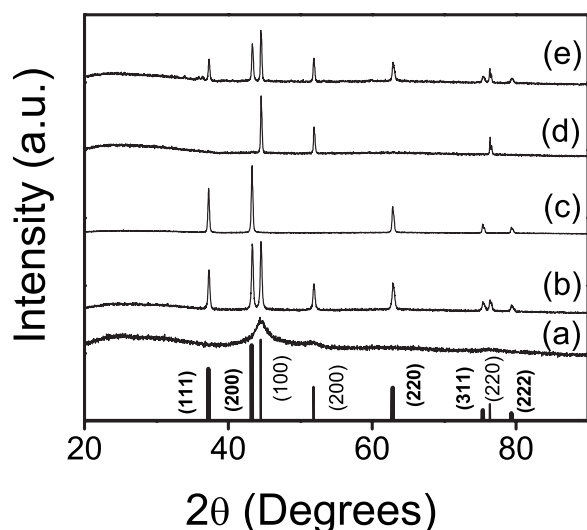
FIG. 2. A comparison of the x-ray powder patterns for different samples. (a) as-prepared Ni protomaterial, (b) Ni protomaterial after oxidizing in air for 3 days at 450 °C, (c) Ni protomaterial after oxidizing in air for 3 days at 900 °C, (d) the faceted Ni nanocrystals, and (e) the faceted Ni nanocrystals after reoxidation at 800 °C. The primary Ni and NiO diffraction peaks are identified according to their values for bulk Ni (black indices) and NiO (bold indices) as reported in the JCPDS database (cards #04–0850 and #78–0423, respectively).

solution was interrupted before they reached the critical size required to sustain true crystallinity.[17,18] This amorphous Ni is an ideal protomaterial, from which we will use high-temperature oxidation and reduction as routes to forming highly crystalline Ni, NiO, and ultimately even composite nanoparticles. Our first experiment involves heating the Ni protomaterial in air, a process which culminates in the formation of highly ordered NiO nanoparticles. TGA and DTA were combined to study the oxidation of the Ni protomaterial. In both cases, 7 mg of material was placed in an alumina crucible, which was subsequently heated at a constant rate of 50 °C/min to the final temperature of 1000 °C. The oxidation process is depicted in the TGA and DTA data presented in Fig. 4. It is known that Ni particles grown by our technique are protected from oxidation at room temperature by the attachment of ethylene-glycol molecules to the particles.[19] The ethylene-glycol molecules dissociate into H_2O, CO_2, and a surface carbonate at 200–250 °C, leading to the gradual weight loss observed in the TGA and the low-temperature peak in DTA, setting the stage for the oxidation of the Ni particles at higher temperatures. The coincidence of the second peak in the DTA with the rapid weight gain in TGA shows that the formation of NiO occurs initially at ~250 °C, and its cessation at ~400 °C likely indicates that the surfaces have been passivated by oxide formation. This is in good agreement with experiments conducted on carefully prepared Ni surfaces, which indicate that oxide layers formed at these low temperatures are limited to only a few unit cells in thickness.[20,21] The formation of crystalline NiO is evident in x-ray diffraction measurements performed after the protomaterial has been oxidized at 450 °C for 3 days [Fig. 2(b)]. Ni and NiO diffraction peaks with similar inten-
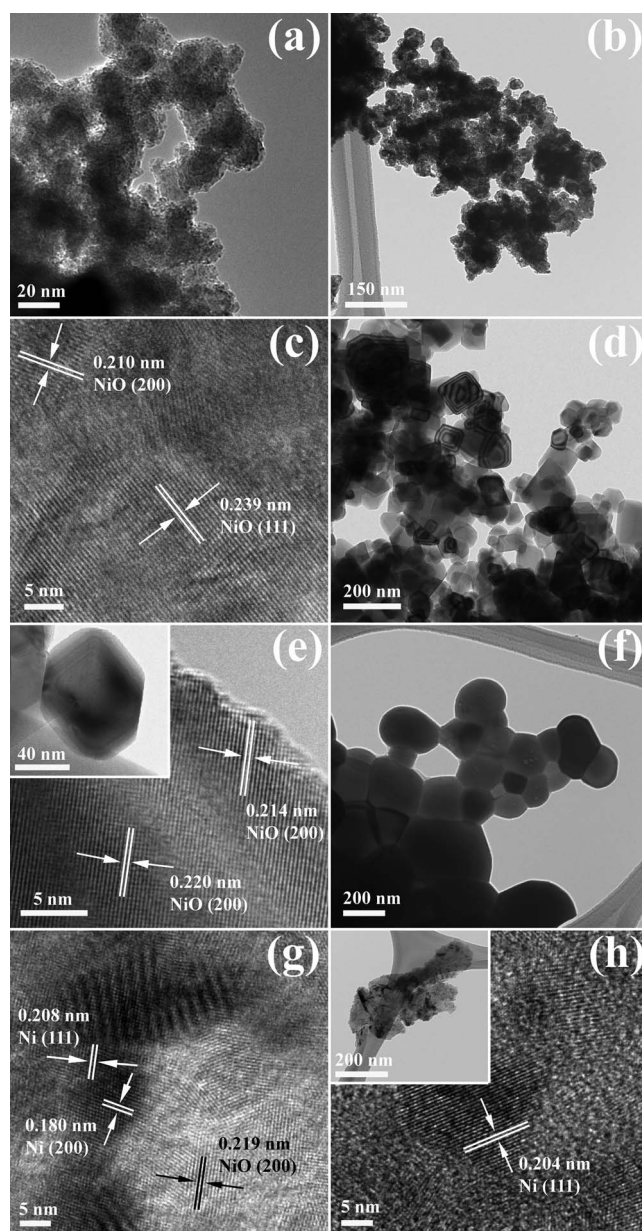
FIG. 3. (a) TEM image of Ni protomaterial. (b) Low-resolution TEM image of Ni protomaterial after oxidizing in air for 3 days at 400 °C. (c) same as (b) but high resolution. (d) Low-resolution TEM image of Ni protomaterial after oxidation at 900 °C for 3 h, (e) same as (d) but high resolution (Inset: closeup of individual NiO nanoparticle). (f) Low-resolution TEM image of faceted Ni nanocrystals prepared by reducing NiO nanocrystals, (g) same as (f) but with high resolution, showing both Ni host and NiO inclusions. (h) Ni protomaterial after a 3 h reduction at 900 °C (Inset: low-resolution image of reduced Ni protomaterial). Length scales are as indicated.

sities are observed. Similar results were observed using an oxidation temperature of 400 °C. Significantly, we see that the Ni and NiO diffraction peaks are as narrow as the resolution of the powder diffractometer, suggesting that the Ni and NiO crystal structures extend over length scales of at least 10 nm. These results imply that there is substantial atomic reorganization at these temperatures, involving the
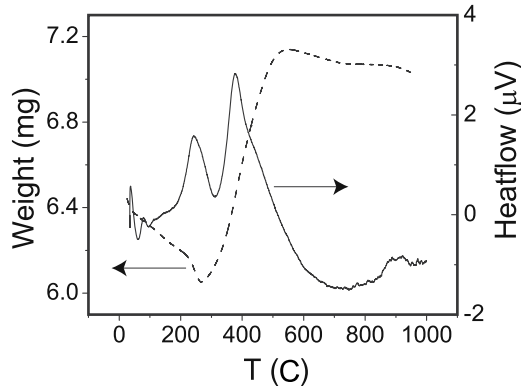
FIG. 4. Results of TGA (left axis, dashed line) and DTA (right axis, solid line) measurements, carried out on Ni protomaterial at a constant heating rate of 50 °C/min.

FIG. 5. Field-dependent magnetization M, normalized to the saturation moment M_S at 10 K of the as-grown Ni protomaterial (solid line) and after a 3 h oxidation at 400 °C (dot-dashed line). Inset: the temperature dependencies of the FC and ZFC magnetizations of the Ni protomaterial oxidized at 400 °C.

motion of both Ni and O atoms. TEM measurements [Figs. 3(b) and 3(c)] provide limited support for this conclusion, showing small NiO crystalline regions embedded in a matrix of indeterminate structure, perhaps best described as the "puddingstone" morphology.

Magnetization measurements confirm the coexistence of Ni and NiO in these lightly oxidized samples. The onset of ferromagnetism is observed below a Curie temperature T_C =750 K, which is substantially enhanced relative to that of bulk Ni, which is 627 K. We believe that strains due to the Ni and NiO lattice-constant mismatch arise at their interface, and as indicated in other measurements,[7,8] these strains are most significant when the oxide overlayer is thin, as in the 400 °C oxidized sample. In many cases, interface strain in thin Ni layers leads to a suppression of T_C,[22,23] however the enhancement of T_C found in our samples suggests instead that the strain is less directional, and acts more like hydrostatic pressure, known to increase T_C in bulk Ni.[24] The relatively smaller Curie temperature in the Ni protomaterial while still enhanced with respect to bulk Ni, can consequently be understood from finite-size scaling[25] as the result of shorter magnetic length scales.

The low-temperature magnetization M is diminished by more than an order of magnitude from its value in the Ni protomaterial, and the maximum in M is shifted from ~100 to ~300 K, indicating a substantial increase in particle size [Fig. 1(a)]. A comparison of the field-cooled (FC) and zero-FC (ZFC) magnetizations, obtained for both with a 1000 Oe measuring field, directly confirms that the dynamics of the lightly oxidized particles occur above room temperature (inset, Fig. 5). Figure 1(b) shows that no direct indication of antiferromagnetic order is observed in $M(T)$, beyond a weak slope change near 400 K. Magnetization loops were obtained at 10 K for both the protomaterial and for the material oxidized at 400 °C for 3 h, and the results are compared in Fig. 5. For the former, a small coercive field H_C= −260 Oe is observed while the latter displays a much larger coercive field H_C=−960 Oe, as well as a loop shift H_{EB} =420 Oe which we interpret as resulting from an exchange-bias effect. The presence of this exchange bias is a clear indication that sufficient crystallinity and magnetic order must exist to define clear-cut interfaces between ferromag-

netic Ni and antiferromagnetic NiO. Similar values of H_{EB} have been observed in another study of Ni/NiO nanoparticle systems.[8]
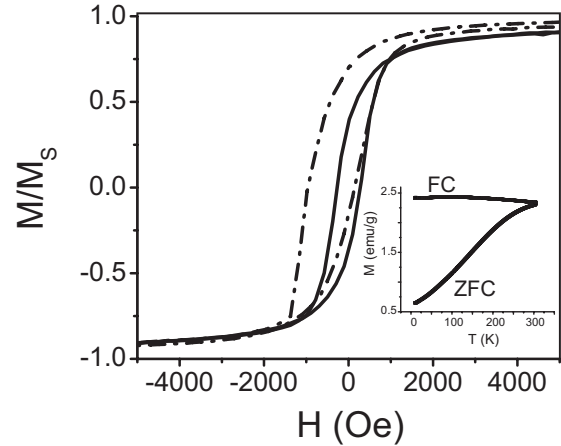
The oxidation process can be brought to completion by continuing it at higher temperatures. TGA measurements (Fig. 4) show that the weight gain increases steadily until ~500 °C, suggesting the near vanishing of elemental Ni. This result is confirmed in Fig. 6(a), which shows the suppression of the 10 K saturation moment M_S, relative to the value $M_{S,0}$ found in the Ni protomaterials, as the material is oxidized for 3 h at progressively higher temperatures. Here, different samples of the protomaterial are heated at 50 °C/min in air from room temperature to the oxidation temperature, where they are held for 3 h before returning to room temperature. Figure 6(a) shows that this procedure results in complete oxidation for temperatures above ~600 °C while Fig. 6(b) shows that holding the sample for 3 h at 900 °C is sufficient to obtain the same result. In agreement with these conclusions drawn from magnetization measurements, only NiO diffraction peaks are observed in the x-ray diffraction experiment performed on material oxidized for 3 days at 900 °C [Fig. 2(c)]. We have refined the powder patterns in the rhombohedral symmetry appropriate for antiferromagnetic NiO,[26–28] and—remarkably—find that the lattice constants and rhombohedral angles are identical to those found in bulk NiO, within our experimental error. No evidence for contaminant phases such as Ni_2O_3 or $Ni(OH)_2$ is found in the powder-diffraction data for any oxidation temperature. Our data indicate that the material which results from high-temperature oxidation of amorphous Ni powder is very similar in structure and stoichiometry to bulk NiO. The morphology of the NiO produced by high-temperature oxidation is revealed in the TEM images presented in Figs. 3(d) and 3(e) for protomaterial which has been oxidized at 900 °C for 3 h. Faceted nanocrystals are formed with typical dimensions which range from 20 to 60 nm. Most of these nanocrystals are hexagonally shaped, with a minority population of cubes observed as well [Fig. 3(d)]. Other research-
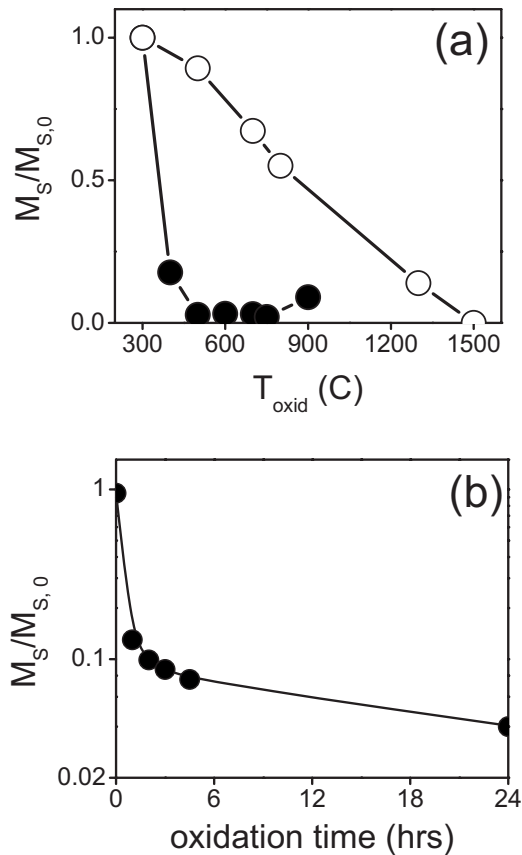
FIG. 6. (a) The reduction in the 10 K saturation moment M_S, normalized to the value measured in the Ni protomaterial $M_{S,0}$ subsequent to 3 h oxidations at different fixed temperatures T_{oxid}. Filled circles are for progressive oxidation of the Ni protomaterial and open circles are for the reoxidation of the faceted Ni nanocrystals. (b) $M_S/M_{S,0}$ measured after oxidation of the Ni protomaterial for different times at 900 °C.

ers have observed faceted Ni nanoparticles, resulting both from syntheses carried out at low temperatures,[29–31] as well as high-temperature molten salt syntheses.[15] Common to all of these synthetic approaches is the high mobility of Ni ions, and it is notable that similar faceting is also observed on bulk Ni surfaces oxidized at temperatures in excess of 900 °C.[32] Unlike the low-temperature syntheses, where this mobility is only possible during the nonequilibrium formation of the nanoparticles themselves, our experiments show that high-temperature treatments can transform amorphous material into crystalline nanoparticles with such high regularity of surfaces that interference effects from the electron beam itself are evident in Fig. 3(d). This perfection persists down to the atomic scale, as the images of atomic planes presented in Fig. 3(e) demonstrate. No defects are evident in these images, although the length scales encompass hundreds of unit cells. Lines of atoms extend in perfect registry to the surface of the nanocrystal itself, which is shown in Fig. 3(e) to be stepped, with the (200) and equivalent crystal planes exposed. This finding is in agreement with experimental findings for bulk Ni surfaces, where it was concluded that the (100) surfaces were most readily oxidized, particularly at high temperature when Ni and O diffusion is unhampered.[20,33–35]
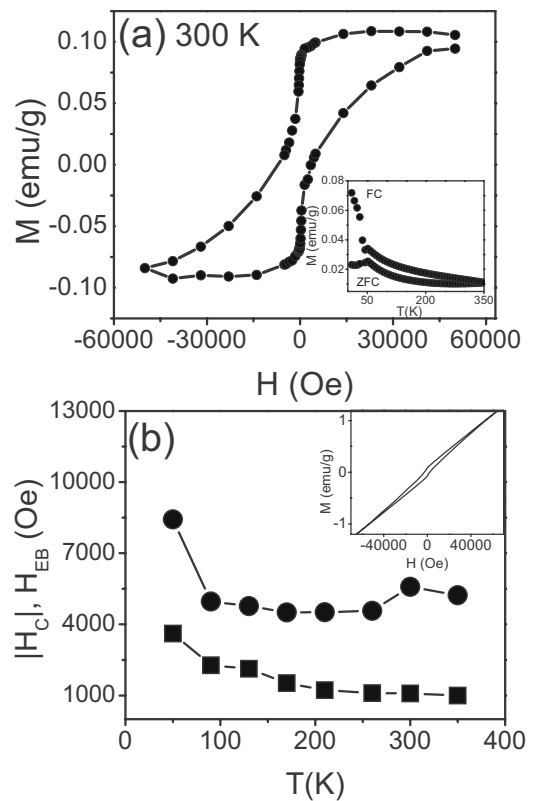
FIG. 7. (a) The saturating part of the magnetization loop of the faceted NiO nanocrystals at 300 K, obtained by subtracting a linear paramagnetic magnetization from the measured $M(H)$. Note the large coercive field H_C and loop shift H_{EB}. Inset: the temperature dependencies of the field-cooled and zero-field-cooled magnetizations. (b) The temperature dependence of H_C (●) and H_{EB} (■). Inset: the as-measured 300 K magnetization loop for the faceted NiO nanocrystals, which were cooled to 10 K in a fixed field of 5 T before the temperature was raised to 300 K for this measurement.

The magnetic properties of these NiO nanocrystals are significantly different from those of bulk NiO. There is no trace in Fig. 1(b) of a ferromagnetic signal in the temperature dependence of the magnetization, consistent with the complete oxidation of the particles. A sharp antiferromagnetic cusp is found in the magnetization near 480 K, indicating that the Néel temperature of the NiO nanocrystals has been reduced by finite-size effects from the bulk value of 523 K. Surprisingly, a second antiferromagnetic transition is observed at ~50 K [see Fig. 1(a)], indicating that the magnetic structure at the lowest temperatures has likely been modified, relative to the bulk magnetic structure.[26–28] Comparing the temperature dependencies of the field-cooled and zero-field-cooled magnetizations, it is evident that the NiO nanocrystals have a net moment which is only blocked below ~350 K, and that the apparent change in magnetic structure found at 50 K further modifies their dynamics [see Fig. 7(a), inset].

Direct evidence that the NiO nanocrystals are moment bearing comes from the field dependence of the magnetization [Fig. 7(a)]. The inset of Fig. 7(b) shows that the magnetization loop is superimposed on a large linear background, is exceptionally broad and does not close, even in fields as large as 14 T. The overall appearance of the magnetization

loop implies that at each field and temperature, there are moments which can be saturated, leading to a closed ferromagnetic loop, and those which are not saturated, which lead to the linear, paramagnetic contribution to the magnetization. The former is plotted in Fig. 7(a) for a fixed temperature of 300 K, clearly showing the presence of a coercive field, $H_C = -5585$ Oe and a loop offset, $H_{EB} = 1000$ Oe. This loop offset increases with decreasing temperature, as shown in Fig. 7(b), exceeding 3500 Oe at 50 K, much larger than the values of H_{EB} found in other core-shell nanoparticle systems.[2–7] Interestingly, there is no obvious change in H_{EB} or H_C near the low-temperature magnetic transition at 50 K, and the loop offset is observed up to the blocking temperature T_B which we infer is at least 350 K. We conclude that the onset of antiferromagnetic order in these NiO particles is quickly followed by the freezing of their dynamics, although the weak FC/ZFC hysteresis reveals the highly frustrated and metastable nature of the antiferromagnetic state. Previous experiments on NiO nanoparticles[8,36–38] find that T_B increases with NiO particle size, and by extrapolating their results, we conclude that a particle diameter larger than 30 nm is required to give $T_B = 350$ K, completely consistent with the range of NiO nanocrystal sizes found in our TEM investigations [Fig. 3(d)]. As has been previously noted,[36–38] the observation of a net moment in NiO is expected, due to surface termination of the antiferromagnetic structure. The broad and open magnetization loop was further explained as the result of multiple sublattice formation,[36] indicating that the lower coordination of the surface moments affects the overall antiferromagnetic structure of the entire nanoparticle, which is much different from that found in a bulk crystal of NiO. Unlike these earlier works, our results indicate that this substructure can be stabilized well above room temperature, and perhaps to the Néel temperature itself, if the host NiO particles are of sufficiently good crystalline quality, and with a large enough volume that the blocking temperature approaches T_N. Despite the large loop offset which can be achieved in large NiO nanoparticles at room temperature, the relatively weak nonlinearity at low fields evident in the raw magnetization loop [inset, Fig. 7(b)] suggests that our NiO nanocrystals will not be useful in their present form as elements of magnetic storage devices. However, it is possible that improved functionality might be realized by using the NiO nanocrystals as a part of ferromagnetic core/antiferromagnetic shell system, where improved control over crystallinity and morphology may yield a large exchange-bias effect at room temperature.[7] A necessary first step to realizing this core-shell morphology is the demonstration that the oxygen in the NiO nanocrystals can be removed and then partially replaced without sustaining significant levels of disorder.

We have succeeded in producing highly crystalline Ni nanoparticles by annealing the NiO nanocrystals in flowing Ar 95%/H 5% at 800 °C for 2 h. We have obtained similar results using high-temperature vacuum annealing, although the time constants are much longer and the uniformity of deoxidation much reduced. X-ray diffraction measurements were carried out on the reduced nanocrystals, and the results are summarized in Fig. 2(d). There is no trace of NiO diffraction peaks, as the powder pattern consists entirely of
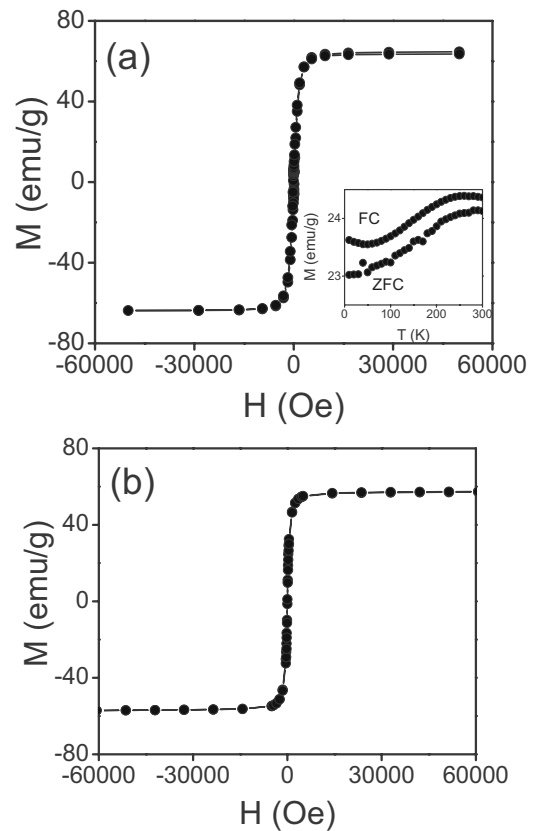
FIG. 8. (a) 10 K Magnetization loop for faceted Ni nanocrystals. Inset: temperature dependencies of the field-cooled and zero-field-cooled magnetizations. (b) same as (a) but after reoxidation at 600 °C.

sharp Ni peaks. The temperature dependence of the magnetization reveals a sharp ferromagnetic transition at 720 K [Fig. 1(b)], and the field-cooled/zero-field-cooled hysteresis in the temperature-dependent magnetization [Fig. 8(a), inset] indicates that the blocking temperature is above 350 K, just as was the case for the faceted NiO nanocrystals. Figure 8(a) demonstrates that the magnetization loop has reverted to an ideal ferromagnetic form, with no measurable coercive field and a saturation value of 65 emu/g, very similar to the value for bulk Ni, 62 emu/g. Finally, TEM measurements reveal that the morphology of NiO nanocrystals is, to some extent, preserved during high-temperature reduction [Figs. 3(f) and 3(g)]. The Ni and NiO particles have similar size distributions and both are faceted instead of spherical. The crystal registry in the faceted Ni nanocrystals is not as high as in the NiO nanocrystals, and the TEM image in Fig. 3(g) shows that there are regions of crystalline NiO present with length scales in the 3–6 nm range. The NiO must be considered a trace remainder of the initial NiO starting material since the x-ray powder patterns do not find an appreciable volume fraction of NiO. Our measurements show that high temperatures are crucial for maintaining the original crystal quality of the faceted NiO nanocrystals post reduction. This is graphically illustrated by a similar attempt to reduce NiO films at much lower temperatures, resulting in a highly disordered and void-filled Ni film.[39] In effect, the cycle of high-temperature oxidation and subsequent reduction to which we

have subjected the amorphous Ni protomaterial has transformed it into the much more desirable and useful form of ordered Ni nanocrystals.

We have investigated whether we might bypass this multistep process and simply generate these faceted and ordered Ni nanocrystals by direct reduction in the Ni protomaterial at high temperatures. The TEM images presented in Fig. 3(h) indicate that this is not possible. While there is substantial coalescence of the particles in the original protomaterial into a polydisperse assemblage of nanoparticles, it is clear that the particles have irregular shapes and inhomogeneous compositions. They are not dissimilar to the materials with short-range order found after low-temperature annealing of the Ni protomaterial depicted in Fig. 3(b). The surfaces themselves are ragged and do not display the clear faceting characteristic of the Ni nanoparticles synthesized by the high-temperature reduction in ideal NiO nanocrystals. We conclude that oxidation is a crucial accompaniment to coalescence in forming highly crystalline NiO nanoparticles from amorphous Ni protomaterial.

The final step toward realizing a ferromagnetic Ni core and antiferromagnetic NiO shell morphology is the oxidation of these Ni nanocrystals. The Ni nanocrystals are subjected to our original oxidation procedure, where they are heated at 50 °C/min to the oxidation temperature, held for 3 h, and then cooled to room temperature. Magnetization loops are subsequently obtained for each sample, and the saturation moment compared to those found during the oxidation of the Ni protomaterial in Fig. 6(a). It is clear that the oxidation of the Ni nanocrystals proceeds much more slowly than that of the protomaterial, perhaps because the former lacks appreciable numbers of defects, known to be highly effective for transporting oxygen to the nanoparticle interior. Indeed, full oxidation of the Ni nanocrystals only occurs as the temperature approaches their melting point, which we determined from DTA to be 1495 °C. Unfortunately, there is no evidence for either a coercive field or an exchange-bias effect in these nanocrystals, at any stage of the reoxidation process. This is a surprising result, especially for samples where the ferromagnetic core is apparently small and the antiferromagnetic shell more than thick enough to control its reorientation. The reason for the absence of an exchange-bias effect became evident once high-resolution TEM measurements were performed.

The TEM experiments reveal that oxidation of the Ni nanocrystals does not result in a conventional core-shell structure. Figure 9 depicts the development of the nanoparticle morphology with increasing oxidation temperature. The faceted nanocrystals persist up to ~600 °C [Fig. 9(a)] but at 700 °C, there is evidence that the smaller nanocrystals are elongating into irregular rods [Fig. 9(b)], not unlike the Ni "sea-urchin" crystals prepared by hydrothermal reduction.[40] After oxidizing at 800 °C, the surface of the nanocrystals has become very rough, and a higher-resolution image shows that nanorods protrude approximately perpendicular to the formerly flat facet of the nanocrystals [Figs. 9(c) and 9(d)]. The nanorods all have similar diameters of ~50 nm, and have lengths which approach the original radius of the underlying nanocrystal. TEM measurements reveal that the nanorods have the same lattice constants as were found in the
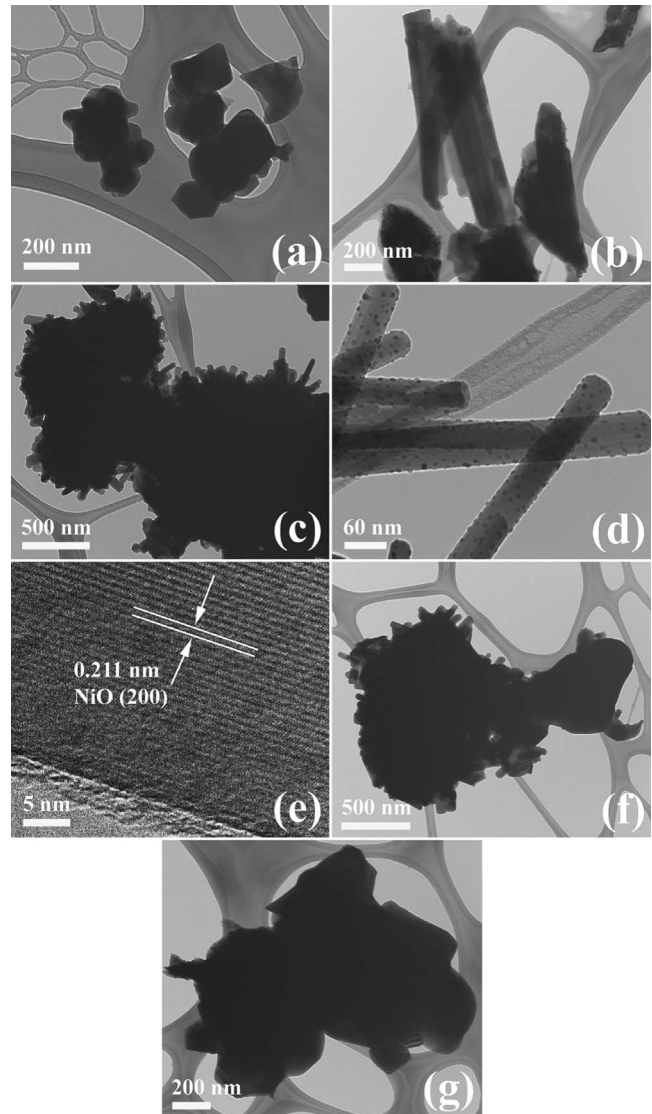
FIG. 9. TEM images illustrating the evolution of the nanoparticle morphology during the reoxidation of the faceted Ni nanocrystals at different temperatures. (a) 600 °C, (b) 700 °C, (c) 800 °C, (d) 800 °C at higher magnification, (e) 800 °C high resolution, (f) 900 °C, and (g) 1300 °C.

faceted NiO nanocrystals [Fig. 9(e)], and accordingly, powder x-ray diffraction measurements performed on these samples [Fig. 2(e)] find sharp Ni and NiO peaks, suggesting that the nanorods arise as a growth instability of the Ni (100) surface. Small islands of a secondary material, perhaps pure Ni, are randomly located on the surface of the nanorods, and the growth ends are hemispherical. It is possible that these islands are introduced during the TEM experiment, if the electron beam has sufficient intensity to sputter material from the sample, which subsequently recondenses on available surfaces as it moves out of the beam. The nanorods grow thicker at 900 °C, and as a result, begin to grow together into a more complex mass [Fig. 9(f)]. As the temperature approaches the melting point, all sharp features on the surfaces of this group of particles are suppressed, and distinct rounding is observed [Fig. 9(g)], presumably as a precursor to melting.

IV. CONCLUSIONS

We have explored here the use of high-temperature oxidation and reduction as ways to prepare highly crystalline materials with the highly directional and ordered interfaces required to optimize exchange-bias effects in Ni/NiO compound nanoparticles. We started with a Ni powder in which minimal crystallinity was observed. No ideal, single-crystalline Ni nanoparticles were present, and we believe that this is because the nucleation of the Ni nanoparticles was interrupted before they reached the critical size required to sustain true crystallinity.[17,18] As this protomaterial is heated, we would expect some degree of coalescence via Ostwald ripening, where the free energy of the particle surface is reduced as large particles grow at the expense of small particles[14] and eventually there should be a population of Ni droplets which are large enough that crystallinity is thermodynamically favored.

One might ask whether the simultaneous oxidation which accompanied coalescence in our experiments is required for particle formation. By heating the Ni protomaterial in a reducing atmosphere of Ar/H, we showed that very poor crystal conformation results, even for extensive high-temperature heat treatment. It is clear that the additional mobility invested in the Ni and O ions by the oxidation process itself is crucial for achieving the highly crystalline NiO nanoparticles which we observe. We speculate that the formation of high quality and homogeneous NiO nanocrystals requires diffusion lengths for the Ni and O ions which approach the size of the nanoparticle itself. For particles in the 20–60 nm range, this requires temperatures above $\sim$600 °C. The net effect of this high ionic mobility is that the particles can self-anneal, and the defects which are inevitably introduced during low-temperature oxidation—otherwise leading to void formation[41]—can now be driven to the surface of the particle and thus expelled. It is striking to note that the surfaces of the NiO nanocrystals are stepped so that the NiO(200) facets are exposed. This is in agreement with previous studies on bulk Ni which found that Ni(100) is the most readily oxidized Ni surface, and that there is an epitaxial relationship which causes NiO (111) to align along the Ni(100) direction.[20,33–35] It is clear that the confluence of particle coalescence, facet formation, and oxidation underlies the formation of the NiO nanocrystals. However successful high-temperature treatments are in forming highly crystalline nanoparticles, it remains an open question whether it is possible to maintain control over the actual size of the nanoparticles themselves, as the coalescence process must continue to temperatures high enough to carry out the self-annealing.

A critical step for using chemical treatments such as oxidation and reduction to construct composite nanoparticles is to demonstrate the reversability of these processes. We have shown that high-temperature reduction in NiO nanocrystals removes the oxygen and creates Ni nanoparticles whose crystallinity is only slightly lower than that of the NiO nanocrystals. Attempts to form the ferromagnetic core/antiferromagnetic shell structure which is optimal for exchange-bias effects in other nanoparticle systems[2–7] by reoxidation were only partially successful. At temperatures below $\sim$700 °C, the core-shell structure was achieved although the oxidation rates were quite low, likely due to the relative scarcity of defects such as voids or grain boundaries which would otherwise transport oxygen efficiently into the nanoparticle interior.[42,43] Since the nanoparticles are quite large, we require a very high degree of oxidation to decrease the core diameter to the point where its dynamics can be controlled by exchange coupling to the antiferromagnetic shell. By extrapolating the low-temperature oxidation rate, it would seem that this degree of oxidation could only occur at temperatures which approached the 1495 °C melting point of the particle itself. However, we found that a novel surface-roughening transition occurs at 800 °C which results in a growth instability of the Ni surface, resulting in the growth of NiO nanorods. While these rods are subsequently melted at higher temperatures, the core-shell structure is never regained, and no exchange-bias effect is observed.

In conclusion, we have shown that it is possible to produce highly crystalline Ni and NiO nanoparticles by exploiting the large ionic mobilities which are present at high temperatures. We have demonstrated that there is a large offset of the magnetization loop measured at room temperature for the NiO nanocrystals. Given the superb crystallinity of these nanoparticles, we can confirm the hypotheses of previous reports[36] that the broad and history-dependent response found in NiO particles is not due to disorder but rather results from a finite-size effect, such as multisublattice formation. Since our process produces NiO nanocrystals which are relatively large, the loop offset is large at room temperature and persists to temperatures which approach the Néel temperature.

Although a motivation for this work was to find a new route to increasing the exchange-bias effect in Ni/NiO composite nanoparticles, an exchange-bias effect was only found during the initial stages of particle formation and oxidation. Unfortunately, the particles are very small at this point, limiting the exchange-bias effect to very low temperatures. Our measurements indicate that there is no stage during particle coalescence and oxidation where the well-defined and highly oriented antiferromagnetic/ferromagnetic interfaces form, making it likely that we never have created the desired core-shell structure during this part of the process. The core-shell structure is realized during the reoxidation of the Ni nanocrystals, at least for temperatures less than $\sim$600 °C, where a surface growth instability occurs. In our particles the Ni core was too large for an appreciable exchange-bias effect with the NiO shell. However, this is not an intrinsic limitation, and it seems likely that a survey of core and shell sizes will identify a suitable range of particle sizes which optimize the exchange-bias effect.

*Author to whom correspondence should be addressed; maronson@bnl.gov

[1] C. Chappert, A. Fert, and F. N. Van Dau, Nature Mater. **6**, 813 (2007).

[2] J. Nogués and I. K. Schuller, J. Magn. Magn. Mater. **192**, 203 (1999).

[3] S. Gangopadhyay, G. S. Hadjipanayis, C. M. Sorensen, and K. Klabunde, J. Appl. Phys. **73**, 6964 (1993).

[4] D. L. Peng, K. Sumiyama, T. Hihara, S. Yamamuro, and T. J. Konno, Phys. Rev. B **61**, 3103 (2000).

[5] V. Skumryev, S. Stoyanov, Y. Zhang, G. Hadjipanayis, D. Givord, and J. Nogués, Nature (London) **423**, 850 (2003).

[6] J. B. Tracy, D. N. Weiss, D. P. Dinega, and M. G. Bawendi, Phys. Rev. B **72**, 064404 (2005).

[7] S. E. Inderhees, J. A. Borchers, K. S. Green, M. S. Kim, K. Sun, G. L. Strycker, and M. C. Aronson, Phys. Rev. Lett. **101**, 117202 (2008).

[8] L. Del Bianco, F. Boscherini, M. Tamisari, F. Spizzo, M. V. Antisari, and E. Piscopiello, J. Phys. D: Appl. Phys. **41**, 134008 (2008).

[9] C. Liu, C. Yu, H. Jiang, L. Shen, C. Alexander, and G. J. Mankey, J. Appl. Phys. **87**, 6644 (2000).

[10] C. Yan, J. Yu, W.-L. Zhou, J.-F. Xie, J.-X. Gao, and D.-X. Zhou, Mater. Sci. Eng., B **99**, 421 (2003).

[11] A. L. Dantas, G. O. G. Reboucase, A. S. Silva, and A. S. Carrico, J. Appl. Phys. **97**, 10K105 (2005).

[12] V. P. Nascimento, E. C. Passamani, A. D. Alvarenga, F. Pelegrini, A. Biondo, and E. Baggio-Saitovich, J. Magn. Magn. Mater. **320**, e272 (2008).

[13] B. B. Nayak, S. Vitta, A. K. Nigam, and D. Bahadur, Thin Solid Films **505**, 109 (2006).

[14] G. Palasantzas, T. Vystavel, S. A. Koch, and J. Th. M. de Hosson, J. Appl. Phys. **99**, 024307 (2006).

[15] Y.-Z. Zheng and M.-L. Zhang, Mater. Lett. **61**, 3967 (2007).

[16] G. G. Couto, J. J. Klein, W. H. Schreiner, D. H. Mosca, A. J. A. de Oliveira, and A. J. G. Zarbin, J. Colloid Interface Sci. **311**, 461 (2007).

[17] Ph. Buffat and J.-P. Borel, Phys. Rev. A **13**, 2287 (1976).

[18] L. F. Cao, G. Y. Xu, D. Xie, M. X. Guo, L. Luo, Z. Li, and M. P. Wang, Phys. Status Solidi B **243**, 2745 (2006).

[19] M. S. Hegde, D. Larcher, L. Dupont, B. Beaudoin, K. Tekaia-Elhsissen, and J.-M. Tarascon, Solid State Ionics **93**, 33 (1996).

[20] W.-D. Wang, N. J. Wu, and P. Thiel, J. Chem. Phys. **92**, 2025 (1990).

[21] T. Okazawa, T. Nishizawa, T. Nishimura, and Y. Kido, Phys. Rev. B **75**, 033413 (2007).

[22] J. R. Childress, C. L. Chien, and A. F. Jankowski, Phys. Rev. B **45**, 2855 (1992).

[23] U. Bovensiepen, P. Poulopoulos, M. Farle, and K. Baberschke, Surf. Sci. **402-404**, 396 (1998).

[24] J. M. Leger, C. Loriers-Susse, and B. Vodar, Phys. Rev. B **6**, 4250 (1972).

[25] G. A. T. Allan, Phys. Rev. B **1**, 352 (1970).

[26] H. P. Rooksby, Acta Crystallogr. **1**, 226 (1948).

[27] W. L. Roth, Phys. Rev. **110**, 1333 (1958).

[28] J. Baruchel, M. Schlenker, and W. L. Roth, J. Appl. Phys. **48**, 5 (1977).

[29] V. Tzitzios, G. Basina, M. Gjoka, V. Alexandrakis, V. Georgakilas, D. Niarchos, N. Boukos, and D. Petridis, Nanotechnology **17**, 3750 (2006).

[30] Y. Chen, D.-L. Peng, D. Lin, and X. Luo, Nanotechnology **18**, 505703 (2007).

[31] H. Winnischofer, T. C. R. Rocha, W. C. Nunes, L. M. Socolovsky, M. Knobel, and D. Zanchet, ACS Nano **2**, 1313 (2008).

[32] R. Peraldi, D. Monceau, and B. Pieraggi, Oxid. Met. **58**, 249 (2002).

[33] E. Kopatzki and R. J. Behm, Phys. Rev. Lett. **74**, 1399 (1995).

[34] Z. Lockman, A. Berenov, W. Goldacker, R. Nast, B. de Boer, B. Holzapfel, and J. L. MacManus-Driscoll, J. Mater. Res. **18**, 327 (2003).

[35] T. G. Woodcock, J. S. Abell, J. Eickemeyer, and B. Holzapfel, J. Microsc. **216**, 123 (2004).

[36] R. H. Kodama, S. A. Makhlouf, and A. E. Berkowitz, Phys. Rev. Lett. **79**, 1393 (1997).

[37] S. A. Makhlouf, H. Al-Attar, and R. H. Kodama, Solid State Commun. **145**, 1 (2008).

[38] E. Winkler, R. D. Zysler, M. V. Mansilla, D. Fiorani, D. Rinaldi, M. Vasilakaki, and K. N. Trohidou, Nanotechnology **19**, 185702 (2008).

[39] A. Matsuda, S. Akiba, M. Kasahara, T. Watanabe, Y. Akita, Y. Kitamoto, T. Tojo, H. Kawaji, T. Atake, K. Koyama, and M. Yoshimoto, Thin Solid Films **516**, 3873 (2008).

[40] X. Liu, X. Liang, N. Zhang, G. Qiu, and R. Yi, Mater. Sci. Eng., B **132**, 272 (2006).

[41] Y. Yin, R. M. Rioux, C. K. Erdonmez, S. Hughes, G. A. Somorjai, and A. P. Alivisatos, Science **304**, 711 (2004).

[42] A. Atkinson, Rev. Mod. Phys. **57**, 437 (1985).

[43] S. Mitra, S. R. Tatti, and J. P. Stark, Thin Solid Films **177**, 171 (1989).